COMMUNICATIONS CHEMISTRY

ARTICLE

DOI: 10.1038/s42004-018-0081-4 OPEN

Biomineralization of calcium phosphate revealed by in situ liquid-phase electron microscopy

Xiaoyue Wang[1], Jie Yang[2], Carmen M. Andrei[3], Leyla Soleymani[2,4] & Kathryn Grandfield[1,2]

Calcium phosphate biomineralization is essential to the formation of bones and teeth, and other pathological calcifications. Unravelling the mechanism of calcium phosphate nucleation and growth contributes significantly to understanding diseases caused by pathological mineralization, and also to designing biomimetic materials with suitable properties. Recently, calcium phosphate was proposed to mineralize following a non-classical crystal growth pathway of pre-nucleation cluster aggregation. Liquid-phase transmission electron microscopy allows dynamic processes to be recorded continuously inside liquid. Here we present direct evidence, based on continuous monitoring in liquid, to confirm that calcium phosphate mineralization from simulated body fluid occurs by particle attachment, shown with nanoscale spatial resolution and sufficient temporal resolution. This work may lay the foundation for future investigation of mineralization in other relevant biological systems in humans and vertebrates.

[1] Department of Materials Science and Engineering, McMaster University, Hamilton L8S 4M1 ON, Canada. [2] School of Biomedical Engineering, McMaster University, Hamilton L8S 4K1 ON, Canada. [3] The Canadian Centre for Electron Microscopy, McMaster University, Hamilton L8S 4K1 ON, Canada. [4] Department of Engineering Physics, McMaster University, Hamilton L8S 4K1 ON, Canada. These authors contributed equally: Xiaoyue Wang, Jie Yang. Correspondence and requests for materials should be addressed to L.S. (email: soleyml@mcmaster.ca) or to K.G. (email: kgrandfield@mcmaster.ca)

Biominerals are diverse natural minerals formed by living organisms. Their elaborate hierarchical structure, distinctive mechanical properties and varied physiological functions have motivated decades of research on their mineralization processes[1,2]. Calcium phosphates (CaP) are one of the most highly researched classes of biominerals, for the reason that the carbonated calcium phosphate apatite crystal is the essential mineral component of both bones and teeth of vertebrates[3]. Also, CaP deposition plays an important role in several pathological calcifications (e.g., arteriosclerosis and physical calculus)[4–6]. Therefore, understanding the mineralization process of CaP will aide in unveiling biomineralization mechanisms of healthy tissues such as bone, dentin and cementum, pathological calcifications (e.g., kidney stones), and also contribute towards research in applied sciences related to human health, such as the development of biomimetic materials and realization of mineralization mechanisms toward synthetic implant systems[5,7].

Currently, the mechanism of CaP nucleation and growth is not fully understood. Based on Cryo-TEM[8] and atomic force microscopy (AFM) studies[9], CaP was suggested to mineralize through complex pathways involving pre-nucleation cluster aggregation, sequential morphological transformations, and finally traversing into the crystalline phase[8–10]. Amorphous calcium phosphate (ACP) has been reported as the transient phase in both in vivo and in vitro studies[11–13]. It has been proposed that the existence of ACP pre-nucleation clusters decreases the energy barrier to nucleation and enables biominerals, such as CaP, to mineralize following a non-classical crystal growth process defined as crystallization by particle attachment[14]. In this process, the pre-nucleation particles, which are regarded as building blocks, are initiated from the solvated state and aggregate with each other to form clusters with chain-like or branched morphology. These pre-nucleation particles could vary from multi-ion complexes to nano-crystals in different mineralization systems[14]. Although these chain-like or branched morphologies of the formed particles captured at defined time points provide important evidence to infer mineralization by attachment-based growth[8,9], they do not directly depict the dynamic formation process. Most studies on crystallization by particle attachment are still based on ex situ observations of crystals made after the pathway of initial nucleation[10]. Therefore, the need arises for a technique to render real-time observation of this dynamic process with nanoscale spatial resolution and necessary temporal resolution[14–16]. While ex situ experiments based on, e.g., cryo-electron microscopy, are excellent for formulating mechanisms, the in situ method developed here is critical for validating these mechanisms through continuous observation in the native liquid environment relevant to biomineralization.

Liquid-phase transmission electron microscopy (LP-TEM), with the ability to record events in confined liquid between two electron-transparent membranes with nanoscale spatial resolution and real-time temporal resolution[17,18], is a promising technique to image dynamic nucleation and growth process of CaP. This approach has been used to study the nucleation and growth of $CaCO_3$[14,15,19] and provides direct experimental evidence for the existence of formation pathways through the transformation of amorphous or crystalline precursors[16]. Also, the dynamic process of calcium ions binding to biopolymers in the formation of metastable amorphous calcium carbonate was recorded via in situ LP-TEM observation[15]. Looking beyond nucleation mechanisms of CaP, the functions of non-collagenous proteins (NCPs)[20] and the collagen matrix[21,22] on crystal nucleation and subsequent growth are also poorly understood. Therefore, in situ TEM research on CaP nucleation and growth could lay a foundation for applying LP-TEM techniques to explore these unsolved issues of bone biomineralization.

A major challenge in using LP-TEM for studying physical and chemical processes is that the electron beam interacts with the liquid sample during imaging. While this is also the case in solid samples, the effect in liquid could lead to more severe consequences due to the high mobility of species in liquid[23]. The beam can charge and move nanoparticles[24], generate bubbles or voids[23], and change the chemistry of the solution by generating reducing and oxidizing species through radiolysis[25]. In spite of these challenges, approaches focused on varying solution chemistry—use of radical scavengers and additives, tuning solution pH, and changing the solvent type—or electron beam conditions—lowering electron dose rate, varying imaging mode, and tuning the accelerating voltage—have shown to be effective in reducing the interference of electron beam with imaging or the process under investigation[26].

In this study, we present real-time imaging of CaP nucleation and growth with in situ LP-TEM, which confirms prior results obtained using cryo-TEM indicating that CaP mineralization occurs by particle attachment.

Results

Liquid-phase TEM for mineralization observations. In order to perform real-time imaging inside the TEM, an in situ scanning LP-TEM system was used to visualize the mineralization process, as shown in the schematic drawing in Fig. 1. The in situ system, composed of two overlapping silicon nitride membranes on silicon chips, confines a limited amount of solution to form a miniaturized cell. The in situ observations were conducted by scanning the focused electron beam across an area of interest where mineralization occurred in a biologically relevant buffer solution, and capturing video of these events.

The free radicals generated through radiolysis of aqueous solution, such as hydrated electrons, $H^{\cdot}$, $OH^{\cdot}$, and so on, can interact with existing active species from solution as reducing and oxidizing agents. These reactions are determined by the concentration of the generated radicals, which are further dependent on the conditions of the microscope and liquid cell, including beam dose rate, solution composition, and temporal and spatial concentration evolution by diffusion and reaction[27]. It has been reported that beam-induced species below a certain concentration result in negligible radiolysis-related reactions[28]. For the system in this study, having a solution with a stable pH of 7.4, a beam dose rate of 21 electrons/frame nm^2 was identified to reduce the beam effect and maintain sufficient spatial resolution at the same time. Furthermore, the beam dose chosen for this in situ study was much lower than the threshold value of beam-induced crystallization reported in previous studies[15]. In addition, the presence of a buffer solution may have contributed to the maintenance of a stable pH which helped to reduce the chemically active species interacting with calcium and phosphate ions contained in the solution to produce beam-induced crystals.

The membranes between which liquid is encapsulated have been reported to bulge[29] due to pressure difference between the liquid inside the cell and the vacuum environment in TEM, as shown encircled in Fig. 1. This bulge contributes to the reduction of the resolution based on an increased thickness of the liquid layer and multiple scattering of the electron beam. In order to reduce the liquid layer thickness and consequently enhance the resolution, the thinnest liquid layer was used (50 nm spacers) and imaging was performed at the corner of a liquid cell where the bulging is minimal. In this study, the bottom chip was patterned with microwells (400 μm × 200 μm each well), which helped to decrease interference between microwells by confining the generated radical species to each well[22,26,29,30]. Based on the in situ setup shown in Fig. 1, a series of in situ studies were

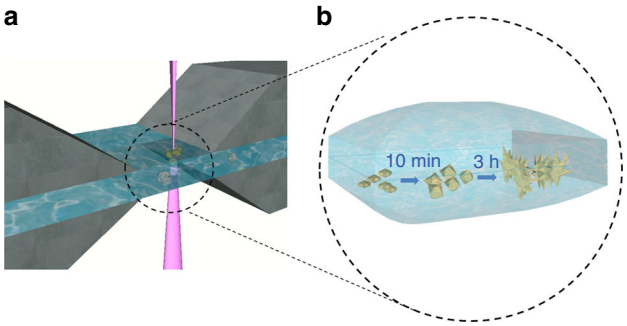

Fig. 1 Schematic of the in situ CaP mineralization process in scanning TEM. The in situ experiment setup is based on the commercialized liquid-cell TEM holder (Poseidon 500, Protochips Inc.). A thin in vitro biomineralization solution layer is sealed by the commercialized chips without spacers to form the static liquid cell, as shown in **a**. This liquid cell contains an electron-transparent window with dimensions of 200 μm × 90 μm for real-time observations. Real-time mineralization process is observed as shown in **b**

performed and followed by characterization and analysis of the products formed.

Real-time observation of the morphological evolution of CaP mineralization. Using in situ scanning LP-TEM, the CaP nucleation and mineralization process was recorded by bright-field (BF) scanning TEM (STEM) with time-resolved and nanoscale spatial resolution (Fig. 2). After a delay of around 2 min, small particles appeared and began increasing in quantity. At around 4 min (Fig. 2b), these particles were clearly discernable and their average diameter measured 10 nm. It was not possible to observe the particles before 2 min due to the limited resolution of the LP-TEM system caused by the scattering of electrons in liquid. These particles had the ability to move and aggregate with each other in solution (Supplementary Movie 1). Initially, they aggregated with the nearby particles to randomly generate branched particle assemblies (Fig. 2c). After the branched assemblies were formed, smaller particles continued to move towards the assemblies and aggregate. With increasing time, these branched assemblies increased in size, and at 14 min aggregated sphere-like particles were obvious (Fig. 2d).

In the images of Fig. 2b–d, we observe two distinct regions. In one region, the particles are clearly resolved, while in the other, they are not resolved or have a very poor resolution. We expect this difference to be due to the presence of a bubble, which reduces the liquid thickness and enhances the imaging resolution in one region. Following this observation, we asked the question: is it likely that the observed aggregation and structural evolution is entirely driven by the bubble formation? Previous liquid microscopy studies have shown that it is possible to study liquid processes in a bubble when a liquid meniscus that wets the surface remains[23]. While the boundary that is formed between the two regions influences the particle accumulation at the edge, it is evident from Supplementary Movie 1 that this boundary does not solely drive the particle aggregation. Throughout the field of view, initially ($t < 10$ min) the particles are moving in all directions and are not solely directed towards the boundary. It should be noted that the influence of the bubble on the process being studied increases at longer exposure times (Supplementary Movie 1) as a larger accumulated beam dose is experienced. Furthermore, the structures that were created under the influence of the electron beam (Fig. 2e) were compared to a beam-blank experiment to validate that the in situ morphology observations were not solely artifacts of the electron beam. A bright-field TEM image of an ex situ synthesized and mineralized sample after 60 min is shown in Fig. 2f with similar particle size and branched assembly morphology. The multi-directional movement of particles during the in situ experiment, along with the similarity in the size and morphology of the structures in the in situ and ex situ experiments indicate that it is unlikely that the observed mineralization experiment is entirely caused by the beam-induced bubble.

The initial morphology evolution observed in situ agrees well with results of cryo-TEM studies on similar CaP systems[8,22]. In those studies, pre-nucleation clusters of calcium triphosphate ions were proposed to exist as the nanometer-sized building blocks for CaP, which decreased the energy barrier for nucleation. These pre-nucleation precursors can aggregate into branched polymeric structures. In many ways, cryo-TEM experiments present advantages over liquid-cell imaging. The established technique often has improved resolution over liquid-cell imaging due to the presence of vitrified ice which scatters the electron beam much less than liquid[31]. This is evident in the case of previous CaP mineralization experiments where particles only 1 nm in size were detected[9] in contrast to those 4–10 nm in size in this study. Soft and beam sensitive materials, particularly organics, are less susceptible to radiolysis damage under cryogenic temperatures as well[31]. In addition, the technique offers versatility via operation as either a 2D or 3D imaging approach with cryo-electron tomography. However, cryo-TEM investigations can only provide morphology evolution according to images at segregated time points of distinct experiments and are unable to record the dynamic mineralization process. In our in situ study, the movement to liquid-cell TEM imaging marks a large improvement in temporal resolution over cryo-TEM. We observed in real-time the nucleation, movement, and morphology evolution of CaP nanoparticles, which provides direct evidence to demonstrate the active mobility of CaP nucleation clusters and supports cryo-TEM findings that show CaP mineralizes by particle attachment[14]. It has been suggested that the CaP pre-nucleation precursor is the initial phase formed during the bone mineralization process to be delivered into the extracellular matrix[11,20]. Here, real-time recording with sufficient temporal and spatial resolution showed the active mobility of initial CaP clusters, which also supports the possibility of their movement towards collagen fibrils in aqueous environments for their eventual mineralization. This work lays the foundation for further investigation of the mediating functions of the extracellular matrix, as well as non-collagenous proteins on CaP mineralization in situ. It is important to note that the reaction kinetics do match those of previous ex situ observations[7,21], which confirms the electron beam effects are not the main driving force of the mineralization processes observed here.

In addition to initial nucleation and growth, it is critical to investigate the particle morphology after longer growth times, since CaP biomineralization involves sequential morphological transformations which could serve as indications of phase changes[9,10]. In the reported in vitro CaP mineralization studies, ribbon-like structures were observed after 3 h[9,32]. In our ex situ mineralization experiment on an E-chip without exposure to the electron beam, the similar flake-like particles were also noted (Fig. 3a). This phase of CaP mineralization was also studied here by another representative in situ TEM experiment shown in Fig. 3b–f. In this experiment, another silicon nitride microchip patterned with discrete microwells was used. After 3 h, the electron beam was moved to a new microwell that had not experienced electron beam exposure and the images in Fig. 3b–f were captured. This enabled the capture of mineralization events after the initial nucleation and growth period of 3 h. This approach assumes that the liquid is confined to each separate

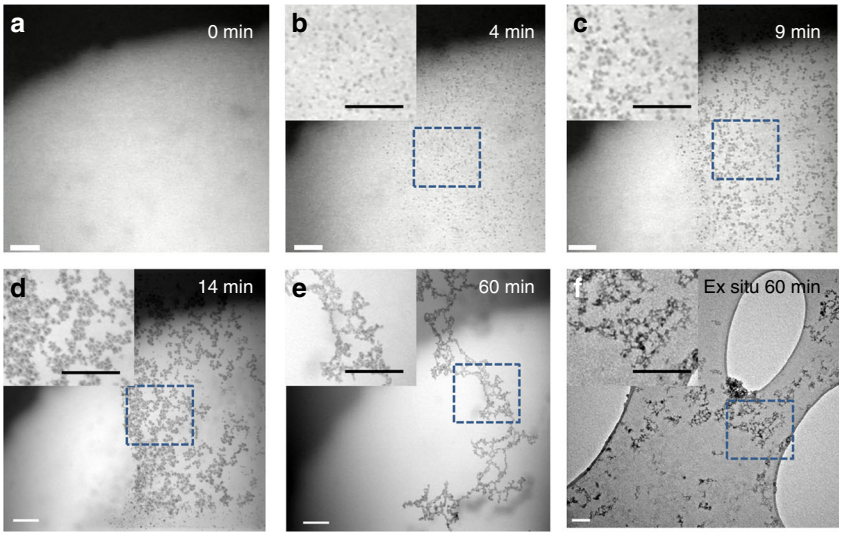

Fig. 2 In situ BF-STEM images showing initial nucleation and growth of CaP over 60 min. **a**–**d** Continuous mineralization from 0 to 14 min, showing the nucleation and growth of CaP particles. **e** Final-branched particle morphology after 60 min. **f** BF-TEM image of ex situ mineralization with similar resulting particle size and morphology after the same growth time. All scale bars represent 200 nm

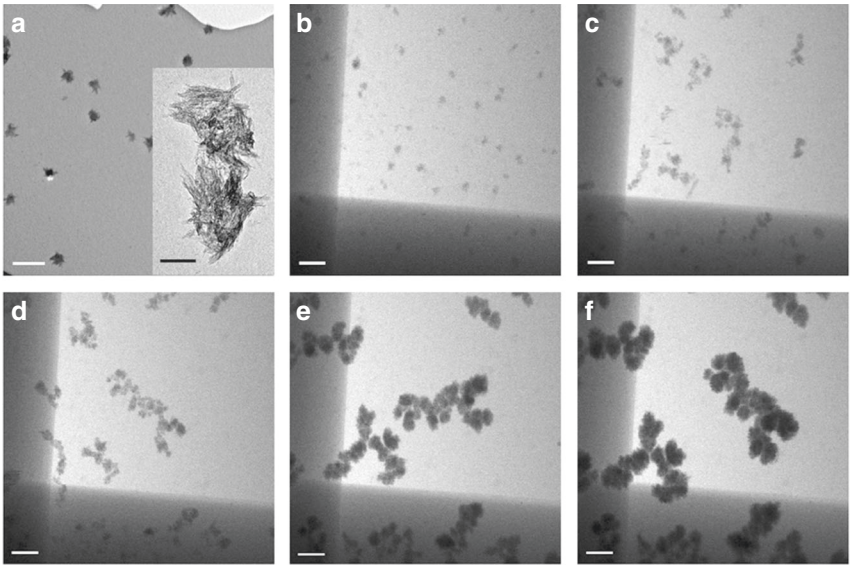

Fig. 3 CaP growth and morphology after 3 h pre-mineralization. **a** BF-TEM images of flake-like particles that resulted after ex situ mineralization on a E-chip without exposure to the electron beam and the inset showing the BF-TEM image of flake-like particles on TEM grid at higher magnification, the scale bar in **a** represents 500 nm and the one for inset represents 100 nm. **b**–**f** Corresponding in situ BF-STEM images showing CaP growth progression after 3 h in a different E-chip from **a**, and recording the growth of dark particles with roughened borders at 0 min (**b**), 1 min (**c**), 2 min (**d**), 6 min (**e**), and 10 min (**f**). All the scale bars in **b**–**f** represent 200 nm

microwell, and therefore, time $t = 3$ h represents growth that was not beam-induced,. Recent works have shown that radiolysis products are largely beam-confined[27] and unlikely to effect a neighboring microwell. Now, sphere-shaped aggregates were observed at time $t = 3$ h (Fig. 3b) and they grew into aggregated assemblies (Fig. 3c, d) during further real-time TEM imaging. Their borders became darker and larger while they rotated within the liquid (Fig. 3e). After around 6 min, the aggregates still had the ability to move by rotation in the liquid, and by 10 min further darkened and grew slightly due to what appears to be conventional crystal growth. It should be noted that while the growth kinetics of particles with and without the electron beam were similar in Fig. 2, when the pre-formed structures (Fig. 3a) were placed under the influence of the electron beam with the available precursors, they grew at a much faster rate. This indicates that the growth of pre-formed structures may be affected more by the presence of the electron beam than the formation and aggregation of nuclei during the initial stage (<60 min), or that the growth kinetics varies at different stages of mineralization. Since the particle morphology from ex situ experiments, shown in Figs. 2f and 3a, so closely matches the events shown in situ after 1 and 3 h, respectively, we can assume that the beam effects on the mineralization pathway are not substantial.

While this work marks a first step towards visualizing CaP mineralization in situ, several technological advances in

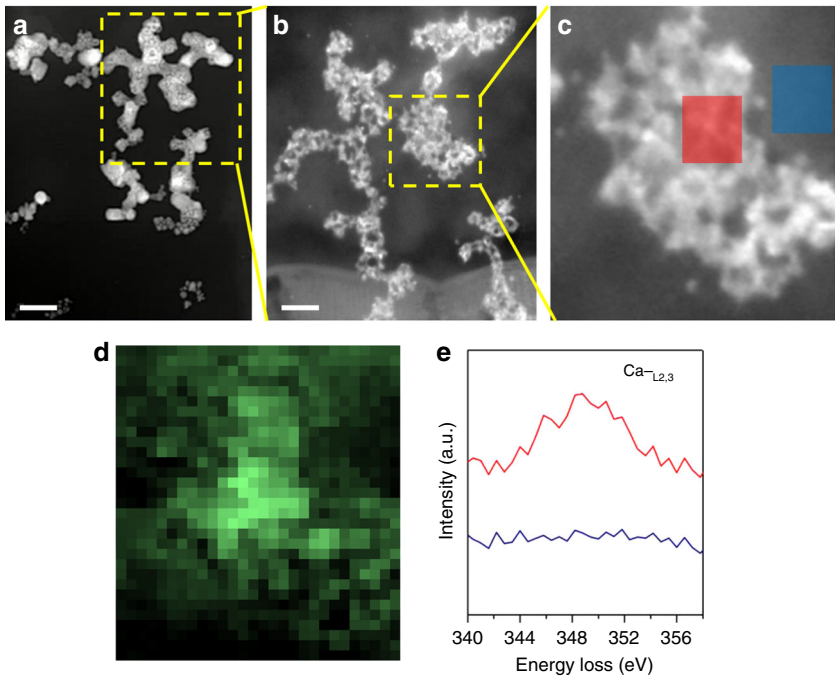

Fig. 4 Post situ characterization of the in situ synthesized particles. **a**–**c** HAADF STEM images of **a** (the scale bar represents 1 µm), the in situ region of interest and **b** (the scale bar represents 50 nm), the same area once the silicon nitride microchips have been opened, and shown at **c**, higher magnification and as **d**, an EELS Ca-map as extracted from the post situ **e**, EELS spectra of the Ca-$L_{2,3}$ edge that demonstrates these particles are Ca-based. The Ca-$L_{2,3}$-edge was identified inside mineralized particles (red), and absent in the surrounding regions (blue)

instrumentation hardware and software could improve this technique for future work. For example, the limited resolution offered in liquid-cell TEM could be improved using advanced direct electron detectors, which collect and essentially amplify electrons from specimens with much weaker signal to noise ratios[33], and by the utilization of sophisticated imaging processing algorithms for signal enhancement[34].

Post situ correlative chemical composition analysis. Due to the relatively thick liquid layer in LP-TEM compared to conventional TEM specimens, spectroscopy characterization in situ is a challenge. Here, we exploited several post situ, or post in situ correlative spectroscopy characterization approaches to probe the mineralization products, specifically X-ray photoelectron spectroscopy (XPS) and electron energy loss spectroscopy (EELS) on the removed in situ chips. This is an essential experiment to validate that the products formed in the microscope are the same products that would form in the absence the electron beam. After the in situ experiment presented in Fig. 1, the silicon nitride microchips were removed from the liquid TEM holder and dried for post situ characterization via XPS. XPS (Supplementary Fig. 1) showed the existence of Ca and P, and the high-resolution spectrum of P contains the peak at 133.89 eV, which matches with the photoelectron line of P in CaP. In addition, the quantitative elemental ratio of XPS analysis showed the Ca/P is ~0.67, which has a nice agreement with the calculated Ca/P ratio range of 0.55 to 0.75 in other studies[9]. This same sample was then probed by EELS, where Fig. 4a and b highlights the region of interest in situ and after drying, respectively. An EELS spectrum image (Fig. 4d) and extracted Ca-$L_{2,3}$ edges (Fig. 4e) confirm the presence of Ca inside mineralized particles and absence in the surrounding regions, which demonstrates these particles are Ca-based. The correlative post situ chemical analyses by XPS and EELS provide strong evidence that the in situ mineralized particles are CaP-based. Also, the Ca/P ratio from the XPS quantitative data reported as 0.67 from the one-hour in situ mineralized sample suggests that the phase of these branched assemblies is not amorphous calcium phosphate (ACP) whose Ca/P ratio is 1.5. ACP was considered as the nanometer-sized building blocks of CaP in other studies[9]. Diffraction pattern is an efficient technique to determine the exact phase of the formed CaP. Due to the large liquid layer and small particle size, obtaining a reliable diffraction pattern in situ to determine the exact phase of the CaP formed was challenging.

Discussion

The real-time observation of CaP mineralization was recorded, which is a direct demonstration that CaP initially mineralizes by particle attachment. Complementary in situ, post situ characterization, and ex situ beam-blank experiments were designed to support this claim. According to post situ TEM-EELS and XPS analysis, the in situ mineralized particles were confirmed to be CaP-based. The samples mineralized in ex situ beam-blank experiments follow similar morphologies as in situ samples, which validates that the in situ morphological observations were not solely artifacts of the electron beam. This study may lay the foundation for further in situ investigation of CaP biomineralization involving more complex organic–inorganic physiological interactions. This paper presents the use of liquid-cell TEM in a calcium phosphate mineralization system. While the resolution is compromised in liquid-cell TEM, it provides real-time tracking of particle aggregation and crystal formation. We also demonstrate the feasibility of investigating biological processes in buffer solutions, which can be used in a variety of biological and mineral research in the future.

Methods

Mineralization solution. The CaP mineralization solution was prepared according to Lausch and co-workers[21,35] who have demonstrated selective remineralization on demineralized murin dentin with this solution. The solution was made up of

two parts: (1) a phosphate solution (9.5 mM Na_2HPO_4 (Sigma Aldrich, USA) in 125 mM NaCl, 50 mM Tris (Sigma Aldrich, USA), pH 7.40), and (2) a calcium solution (1.7 mM $CaCl_2$ in 125 mM NaCl, 50 mM Tris, pH 7.40). All reagents were purchased from Sigma Aldrich and dissolved in Milli-Q water. These two solutions were mixed and filtered through a 0.2 µm acrodisc syringe filter right before sealing in the liquid TEM holder for in situ experiments or placing in the beakers for ex situ experiments at room temperature.

In situ STEM. The in situ TEM holder (Poseidon 500, Protochips Inc., Raleigh, NC, USA) used in this study contains a liquid cell placed at the holder tip. Two microfabricated silicon nitride microchips with 50 nm silicon nitride membranes were sealed inside the liquid cell and in situ imaging was performed by electrons passing through the overlapped silicon nitride membranes. A small amount (2 µl) of CaP mineralizing solution was put in between the two membranes, one of which was patterned with microwells, which assists in maintaining a relatively stable solution during the in situ mineralization process, and reducing beam effect interference between the individual microwells. The E-chips used in this study were commercially available bottom large chips (ETP-42A1, Protochips Inc., Raleigh, NC, USA) containing an 8 × 16 array of 10 µm × 10 µm microwell on a 400 µm × 200 µm SiN membrane and top chips of 300 µm × 90 µm SiN membrane without spacers (ECB-39A, Protochips Inc., Raleigh, NC, USA). Real-time imaging was performed using a JEOL 2010F TEM operated at 200 kV. Bright-field scanning transmission electron microscopy (BF-STEM) mode was used under beam dose of 2.198×10^3 e/Å^2 s. In situ images were acquired using DigiScan II (Gatan, model 788) unit with a BF detector with time resolution of 0.555 s/frame. The whole in situ process was recorded by a CCD camera and series of in situ images were either extracted from the in situ video or captured every 4 s by blanking the electron beam in between.

Post situ and ex situ TEM. To confirm mineralization products formed were similar to those formed without the interaction of any electron beam, so-called ex situ experiments were performed completely outside of the TEM. To confirm 1 h experiments, mineralization products were acquired by dropping dispersed mineralized solution after 1 h onto carbon-coated TEM copper grids followed by immersion in methanol to halt any further particle development. For the confirmation of products after 3 h under confinement, the same amount of CaP mineralization solution (0.2 µl) was sealed inside the in situ TEM liquid cell for 3 h, but not placed under the electron beam. The E-chips were then taken out, washed with methanol to terminate further mineralization, and viewed in the TEM.

After the in situ experiment, the E-chips were removed from the liquid TEM holder, separated and then dried for further post situ characterization. The post situ experiments were conducted sequentially, with XPS performed first (detailed below), and EELS performed after mounting the sample onto a molybdenum grid to mount on a standard double-tilt holder. As for all experiments, a JEOL 2010F TEM with the accelerating voltage of 200 kV was employed to characterize the post situ mineralized samples on the dried E-chips, as well as the ex situ mineralized samples above in both TEM and STEM bright-field imaging modes, and by STEM-EELS. Principle component analysis (PCA) was used to decrease noise in the Ca elemental distribution EELS map.

X-ray photoelectron spectrometry. Both in situ mineralized samples on the dried E-chips and ex situ mineralized samples on TEM grids were characterized by an imaging and scanning X-ray photoelectron spectrometer (XPS) (PHI Quantera II, Physical Electronic, MN). The time-dependent ex situ mineralized samples were prepared by spin-coating dispersed mineralized solution onto cleaned silicon wafer substrates and then immersing them in methanol to wash away NaCl. All the selected regions of interest were scanned by monochromated Al Kα (280 eV) with 5 sweeps for 200 micron beam (50 power) and 20 sweeps for 7.5 micron beam (0.8 W power). 55 eV pass energy scanning with 200 micron beam and 120 sweeps was used for the P1s high-resolution spectra. Dual beam neutralization was used to prevent samples from charging. Calibration was done using a clean piece of silver foil.

Data availability

The data that support the findings of this study are available from the corresponding author upon request.

Received: 11 July 2018 Accepted: 18 October 2018
Published online: 13 November 2018

References

1. Weiner, S. & Dove, P. M. An overview of biomineralization processes and the problem of the vital effect. *Rev. Mineral. Geochem.* **54**, 1–29 (2003).
2. Addadi, L. & Weiner, S. Biomineralization: mineral formation by organisms. *Phys. Scr.* **89**, 098003 (2014).
3. Dorozhkin, S. V. Calcium orthophosphates in nature, biology and medicine. *Materials* **2**, 399–498 (2009).
4. Guangbin, L. et al. Spontaneous calcification of arteries and cartilage in mice lacking matrix GLA protein. *Nature* **386**, 78–81 (1997).
5. Dorozhkin, S. V. & Epple, M. Biological and medical significance of calcilum phosphates. *Angew. Chem. Int. Ed.* **41**, 3130–3146 (2002).
6. Yiu, A. J., Callaghan, D., Sultana, R. & Bandyopadhyay, B. C. Vascular calcification stone disease: a new look towards the mechanism. *J. Cardiovasc. Dev. Dis.* **2**, 141–164 (2015).
7. Wang, X. et al. Biomineralization at titanium revealed by correlative 4D tomographic and spectroscopic methods. *Adv. Mater. Interfaces* **1800262**, 1–9 (2018).
8. Dey, A. et al. The role of prenucleation clusters in surface-induced calcium phosphate crystallization. *Nat. Mater.* **9**, 1010–1014 (2010).
9. Habraken, W. J. E. M. et al. Ion-association complexes unite classical and non-classical theories for the biomimetic nucleation of calcium phosphate. *Nat. Commun.* **4**, 1507 (2013).
10. Van Driessche, A. E. S., Kellermeier, M., Benning, L. G. & Gebauer, D. *New Perspectives on Mineral Nucleation and Growth* (Springer, Cham, 2017).
11. Nudelman, F., Lausch, A. J., Sommerdijk, N. A. J. M. & Sone, E. D. In vitro models of collagen biomineralization. *J. Struct. Biol.* **183**, 258–269 (2013).
12. Mahamid, J. et al. Mapping amorphous calcium phosphate transformation into crystalline mineral from the cell to the bone in zebrafish fin rays. *Proc. Natl Acad. Sci. USA* **107**, 6316–6321 (2010).
13. Boonrungsiman, S. et al. The role of intracellular calcium phosphate in osteoblast-mediated bone apatite formation. *Proc. Natl Acad. Sci. USA* **109**, 14170–14175 (2012).
14. De Yoreo, J. J. et al. Crystallization by particle attachment in synthetic, biogenic, and geologic environments. *Science* **349**, aaa6760–aaa6760 (2015).
15. Smeets, P. J. M., Cho, K. R., Kempen, R. G. E., Sommerdijk, Na. J. M. & De Yoreo, J. J. Calcium carbonate nucleation driven by ion binding in a biomimetic matrix revealed by in situ electron microscopy. *Nat. Mater.* **14**, 394–399 (2015).
16. Nielsen, M. H., Aloni, S. & De Yoreo, J. J. In situ TEM imaging of $CaCO_3$ nucleation reveals coexistence of direct and indirect pathways. *Science* **218**, 213–218 (2013).
17. De Jonge, N. & Ross, F. M. Electron microscopy of specimens in liquid. *Nat. Nanotechnol.* **103**, 695–704 (2011).
18. Ross, F. M. Opportunities and challenges in liquid cell electron microscopy. *Science* **350**, 1–9 (2015).
19. Verch, A., Morrison, I. E. G., Van De Locht, R. & Kröger, R. In situ electron microscopy studies of calcium carbonate precipitation from aqueous solution with and without organic additives. *J. Struct. Biol.* **183**, 270–277 (2013).
20. Olszta, M. J. et al. Bone structure and formation: a new perspective. *Mater. Sci. Eng. R. Rep.* **58**, 77–116 (2007).
21. Lausch, A. J., Quan, B. D., Miklas, J. W. & Sone, E. D. Extracellular matrix control of collagen mineralization in vitro. *Adv. Funct. Mater.* **23**, 4906–4912 (2013).
22. Nudelman, F. et al. The role of collagen in bone apatite formation in the presence of hydroxyapatite nucleation inhibitors. *Nat. Mater.* **9**, 1004–1009 (2010).
23. Grogan, J. M., Schneider, N. M., Ross, F. M. & Bau, H. H. Bubble and pattern formation in liquid induced by an electron beam. *Nano Lett.* **14**, 359–364 (2014).
24. White, E. R., Mecklenburg, M., Shevitski, B., Singer, S. B. & Regan, B. C. Charged nanoparticle dynamics in water induced by scanning transmission electron microscopy. *Langmuir* **28**, 3695–3698 (2012).
25. Zhu, G. Z. et al. In situ liquid cell TEM study of morphological evolution and degradation of Pt-Fe nanocatalysts during potential cycling. *J. Phys. Chem. C* **118**, 22111–22119 (2014).
26. Woehl, T. J. & Abellan, P. Defining the radiation chemistry during liquid cell electron microscopy to enable visualization of nanomaterial growth and degradation dynamics. *J. Microsc.* **265**, 135–147 (2017).
27. Schneider, N. M. et al. Electron-water interactions and implications for liquid cell electron microscopy. *J. Phys. Chem. C* **118**, 22373–22382 (2014).
28. Woehl, T. J. et al. Ultramicroscopy experimental procedures to mitigate electron beam induced artifacts during in situ fluid imaging of nanomaterials. *Ultramicroscopy* **127**, 53–63 (2013).
29. Holtz, M. E., Yu, Y., Gao, J., Abruña, H. D. & Muller, Da In situ electron energy-loss spectroscopy in liquids. *Microsc. Microanal.* **19**, 1027–1035 (2013).
30. Schneider, N. M. in *Liquid cell electron microscopy* (ed. Ross, F. M.) 140–163 (Cambridge University, New York, NY, 2017).
31. Patterson, J. P., Xu, Y., Moradi, M. A., Sommerdijk, N. A. J. M. & Friedrich, H. CryoTEM as an advanced analytical tool for materials chemists. *Acc. Chem. Res.* **50**, 1495–1501 (2017).

32. Nitiputri, K. et al. Nanoanalytical electron microscopy reveals a sequential mineralization process involving carbonate-containing amorphous precursors. *ACS Nano* **10**, 6826–6835 (2016).
33. Taheri, M. L. et al. Current status and future directions for in situ transmission electron microscopy. *Ultramicroscopy* **170**, 86–95 (2016).
34. Schneider, N. M., Park, J. H., Norton, M. M., Ross, F. M. & Bau, H. H. Automated analysis of evolving interfaces during in situ electron microscopy. *Adv. Struct. Chem. Imaging* **2**, 2 (2017).
35. Deshpande, A. S. Bioinspired synthesis of mineralized collage fibrils. *Cryst. Growth Des.* **8**, 3084–3090 (2008).

Acknowledgements

K.G. acknowledges financial support from the Discovery Grant program of the Natural Sciences and Engineering Research Council of Canada (NSERC). L.S. acknowledges financial support from the Natural Sciences and Engineering Research Council of Canada and the Canada Research Chair program. X.W. acknowledges support from the Ontario Trillium Scholarship. Electron microscopy was performed at the Canadian Centre for Electron Microscopy (CCEM), a facility supported by the Canada Foundation for Innovation under the Major Science Initiative program, NSERC, and McMaster University. Gianluigi Botton, the scientific director of CCEM, is gratefully acknowledged for his continued support and guidance.

Author contributions

X.W. and J.Y. performed the in situ experiments. X.W. performed the ex situ experiments and analyzed data. C.A. performed the EELS experiments and analyzed the data with X. W. X.W., J.Y., L.S., and K.G. contributed to writing the manuscript.

Additional information

Supplementary Information accompanies this paper at https://doi.org/10.1038/s42004-018-0081-4.

Competing interests: The authors declare no competing interests.

Reprints and permission information is available online at http://npg.nature.com/reprintsandpermissions/

Publisher's note: Springer Nature remains neutral with regard to jurisdictional claims in published maps and institutional affiliations.